Title

Erosional cascade during the 2021 Melamchi Flood

Author list

Chan-Mao Chen [1, *], James Hollingsworth [2], Marin K. Clark [3], Deepak Chamlagain [4], Sujata Bista [4], Dimitrios Zekkos [5], Anuj Siwakoti [4], A. Joshua West [1]

Affiliations

[1] Department of Earth Sciences, University of Southern California, Los Angeles, CA, USA

[2] Université Grenoble Alpes, Université Savoie Mont Blanc, CNRS, IRD, Université Gustave Eiffel, ISTerre, 38000 Grenoble, France

[3] Department of Earth and Environmental. Sciences, University of Michigan, Ann Arbor, MI, USA

[4] Department of Geology, Tri-Chandra Multiple Campus, Tribhuvan University, Kathmandu, Nepal

[5] Department of Civil and Environmental Engineering, University of California at Berkeley, Berkeley, CA, USA

* Corresponding author: chanmaoc@usc.edu

Abstract

In 2021 a catastrophic flood occurred in the Melamchi Valley of Nepal, causing widely distributed erosion in Himalayan headwaters and mobilizing a large sediment volume. As the flood progressed downstream it induced an erosional cascade, producing 100m deep incisions into high-elevation valley fills, generating new landslides, and burying the lower reaches in alluvium. This event demonstrated the destructive impact of cascading processes and their potential for reshaping the landscape.

Main text

Large, sediment-laden “debris floods” can have disastrous consequences in mountainous terrain [1,2]. The frequency of these devastating floods and the extent of their impacts are likely to grow in the future [3]. Knowledge of flood formation mechanisms and dynamics is critical for hazard management [4], and for evaluating their role in landscape evolution and carbon transport [5,6]. Because debris floods move large amounts of sediment [7], they typically cause dramatic erosion and deposition along river valleys. These changes can contribute substantially to flood damage, e.g., undermining some buildings and burying others. Topographic change can also retain

information about the event itself. Here, we use a time-series of high-resolution topographic models to illuminate the complex interactions that generated the 2021 Melamchi Flood in the central Himalaya of Nepal. This approach reveals the "cascading" nature of this event, with implications for the origin and impact of other floods in mountainous regions.

The Melamchi Flood occurred in central Nepal, where topography changes from subdued foothills in the south to high mountains in the north associated with a pronounced gradient in rock uplift and exhumation driven by Himalayan tectonics (Fig. 1a; Extended Data Fig. 1). This region experienced intense landsliding during the 2015 Mw7.8 Gorkha Earthquake [8]. The 2021 flood initiated with intense monsoon rainfall (15 mm/hr) on June 14, accompanied with strong snowmelt [9]. Peak discharge on June 15 at Nakote was estimated to be 7162 m^3/s [10], similar to recent major Himalayan outburst floods [2,4]. The Melamchi Flood claimed 25 lives, destroyed hundreds of buildings, and damaged the Melamchi Water Supply Project (MWSP) which was designed to supply 170 million liters to Kathmandu per day. Two other large floods followed on July 31, 2021, and August 11, 2023, exacerbating the damage. The June 2021 flood was associated with breaching of a glacial lake, numerous landslides, and multiple areas of erosion and deposition [9,11,12]; however, how these elements were connected and the roles they played in the flooding process are still to be fully understood.

We use topographic change detection across the entire Melamchi watershed to piece together the cascade of processes that generated the 2021 event and to track subsequent evolution. Using very high-resolution (50 cm) optical satellite imagery from between 2014 and 2023, we mapped areas of visible change, produced a time series of 1-m resolution stereo-photogrammetric digital surface models (DSMs), and quantified the volumes of erosion and deposition (see Methods). We capture changes associated with the 2015 Gorkha Earthquake, the 2021 Melamchi Flood, and the monsoonal floods of 2022-23.

Our analysis shows that vast amounts of sediment were evacuated from low-order headwaters during the 2021 event. Hillslope gullies incised tens of meters deep, moraines collapsed in several locations (up to 40 m; Extended Data Fig. 2), and numerous old landslides were reactivated due to channel undercutting. These processes were observed among all headwater basins, suggesting widely distributed erosion in the early stage of flood formation (Fig. 1a). The Pemdang Khola accounted for three quarters of the headwater sediment output, likely due to the most intense snowmelt [9], plus breaching of a small glacial lake (Extended Data Fig. 2). Links

between the 2015 Gorkha Earthquake and mass wasting in this headwater area during the 2021 flood remain enigmatic. Our mapping suggests only 6-9% of the Gorkha Earthquake-associated landslides were reactivated during the flood, consistent with prior suggestions that flood erosion was mostly new [12]. However, the earthquake legacy may have played a role by weakening the substrate [13].

Of the 6.334 Mm^3 sediment delivered from the low-order headwaters, 5.382 Mm^3 was deposited on the wide valley at Bremathang (3600 m elevation; Extended Data Fig. 3), aggrading the 0.5 × 2 km plain by 5-10 m with boulder-rich sand (see field photos in Extended Data Fig. 4). This low relief plain perched within the High Himalaya consists of sediments trapped behind a long-lived natural dam system, likely created by a combination of peri-glacial processes and valley-blocking landslides. During the flood, it appears that this dam system was broken as its "boulder armor" (visible in pre-flood satellite imagery and relict dam surfaces in the field) was removed (Extended Data Fig. 4). The flood cut into the relatively weak interior of the Bremathang deposit by more than 100 m. As a result, 48.62 Mm^3 of material was released from a 3.8 km-long stretch, serving as the largest sediment source in this event (Fig. 1b, 2). In total, within the headwater basins (134 km^2 area) that saw greatest erosion, 50.527 Mm^3 was removed, equivalent to 67-157 years of erosion at the estimated long-term rate of 2.4-5.6 mm/yr [14].

Taking advantage of steep confined channels in the middle reaches, most material from Bremathang was transported efficiently to the lower basin during flooding. Along the way, undercutting of slopes by river incision (10-20 m riverbed lowering in many places) caused several large landslides that contributed additional sediment (Extended Data Fig. 5). The largest landslide occurred below Melamchi Ghyang Village, where ~6 Mm^3 of material slumped into the river and blocked flow for ~45 minutes [9]. Slope stability analysis suggests that the incision we measure (15-21 m) would have been sufficient to cause this failure (Extended Data Fig. 6). Although this landslide was not the primary sediment source for the Melamchi Flood as a whole, the associated damming and release may have magnified the downstream damage, emphasizing the role of multiple connected processes in this cascade.

Large-scale aggradation (4-23 m) and 2- to 6-fold channel widening (from ~30-60 m to ~100-300 m) occurred when the flood arrived in the lower reaches (Fig. 3b-c), where river channel slopes are <2.5°. We observed numerous boulders in flood deposits. In most deposits, the largest boulders were 1-2 m in diameter, but some were 5-10 m (Fig. 3d) — confirming this event as a

"debris flood" (*sensu* Church and Jakob, 2020 [7]). Hydraulic calculations suggest the largest boulders could not all have been moved by shear stress exceedance considering flow depths from model reconstructions [10] and evidence from flood markers on buildings [15] (see Extended Data Fig.7-8; Methods). These results imply that other mechanisms were also likely at work in the Melamchi Flood, such as momentum transfer by grain-grain collision [16], turbulence generation [17], and support by high concentration of suspended load [18].

Based on our 2021 sediment budget, the total flood-induced erosion within the Melamchi catchment was 75.823 Mm^3. Most of this material came from pre-existing sediment trapped at Bremathang, although we observed some new bedrock erosion, especially in the middle reaches. Compared to the much larger erosion volume, deposition within the Melamchi Khola basin was 22.681 Mm^3 (Fig. 1b). Thus 53.142 Mm^3 of material (70% of the total flood erosion volume) was delivered further downstream during the 2021 flood. Moreover, of the 16.249 Mm^3 sediment that was deposited in 2021 within the lower reaches of the Melamchi valley, more than 1.067 Mm^3 sediment was removed as of 2023, indicating efficient evacuation of the flood debris as this part of the system shifted from aggradation (during the 2021 flood) to erosion (in following monsoon seasons).

Altogether, the sediment erosion and deposition that we quantify in this study record the progression and impact of the Melamchi Flood, illuminating the interaction of multiple processes and sediment sources (Fig. 3a). We document dramatic and widely distributed headwater erosion, revealing that the Melamchi Flood was more than a single outburst event. This inference would be difficult to make from other observations (e.g., downstream river levels) alone. The flood developed into an unfolding disaster as it progressed downstream. Dramatic erosion of deposits at Bremathang, which contributed 64% of the total eroded material, highlights the importance of understanding sediment accumulation in the Himalayan uplands over earthquake and climatic cycles [19]. Further erosion of the Bremathang deposits in 2023 (Fig. 2) followed removal of the boulder armoring in 2021, such that future monitoring of this area will be critical for hazard assessment in the Melamchi-Indrawati Basin, and for the future of the MWSP. Additional contributions to the flood from slope failures such as at Melamchi Ghyang show the role of hillslope-channel coupling and the potential for dam formation via slope undercutting, followed by subsequent breaching, to magnify flood impacts. Quantifying aggradation in the lower reaches allows evaluation of long-lasting effects including future inundation during monsoonal rains.

Based on lessons learned from the Melamchi Flood, projection of future extreme floods should account for not just the role of single-source outburst events, which are increasingly recognized as cause of concern in mountainous areas [1,2,4], but also should consider how the complex interactions along a flood path may produce a "cascading effect" that begins with heavy precipitation over headwaters and gradually develops downstream. The "long tail" of such a cascade can persist even years later, as we see in 2023. Thus, characterizing multiple sediment sources will be vital to anticipating future flood hazard in mountainous settings. Moreover, past floods such as the Melamchi event may complicate the interpretation of basin-filling deposits as definitively related to past earthquakes [20]. Finally, the Melamchi Flood redistributed a considerable mass (>75 million m^3) from steep headwaters to gentle lowlands; such events play important roles as efficient agents of erosion and sediment evacuation, and therefore in the landscape evolution of the Himalaya.

Acknowledgement

This work is supported by the US NSF Frontier Research in Earth Sciences program awards 2021619 to AJW, 2020970 to MKC, and 2021299 to DZ. We thank Josh Roering, Kristen Cook, Jakob Steiner, Amaury Dehecq, and Gen Li for helpful discussions, and Bhairab Sitaula and Harka Tamang for field assistance. We thank the Department of Mines and Geology (DMG) and the Department of Hydrology and Meteorology, Government of Nepal, for the fieldwork permission, guidance, and rainfall data collection. Pléiades images (©CNES, 2023; distribution Airbus) were obtained via the DINAMIS platform.

Author Contributions Statement

A.J.W., C.M.C., M.K.C., D. Z., and D.C. conceived the study. All authors contributed to study design. C.M.C., A.J.W., and J.H. performed the remote-sensing analyses. C.M.C., S.B., and A.S. collected the field data. C.M.C. and A.J.W. interpreted the data and wrote the manuscript with contributions from all co-authors.

Competing Interests Statement

The author declares no competing interests.

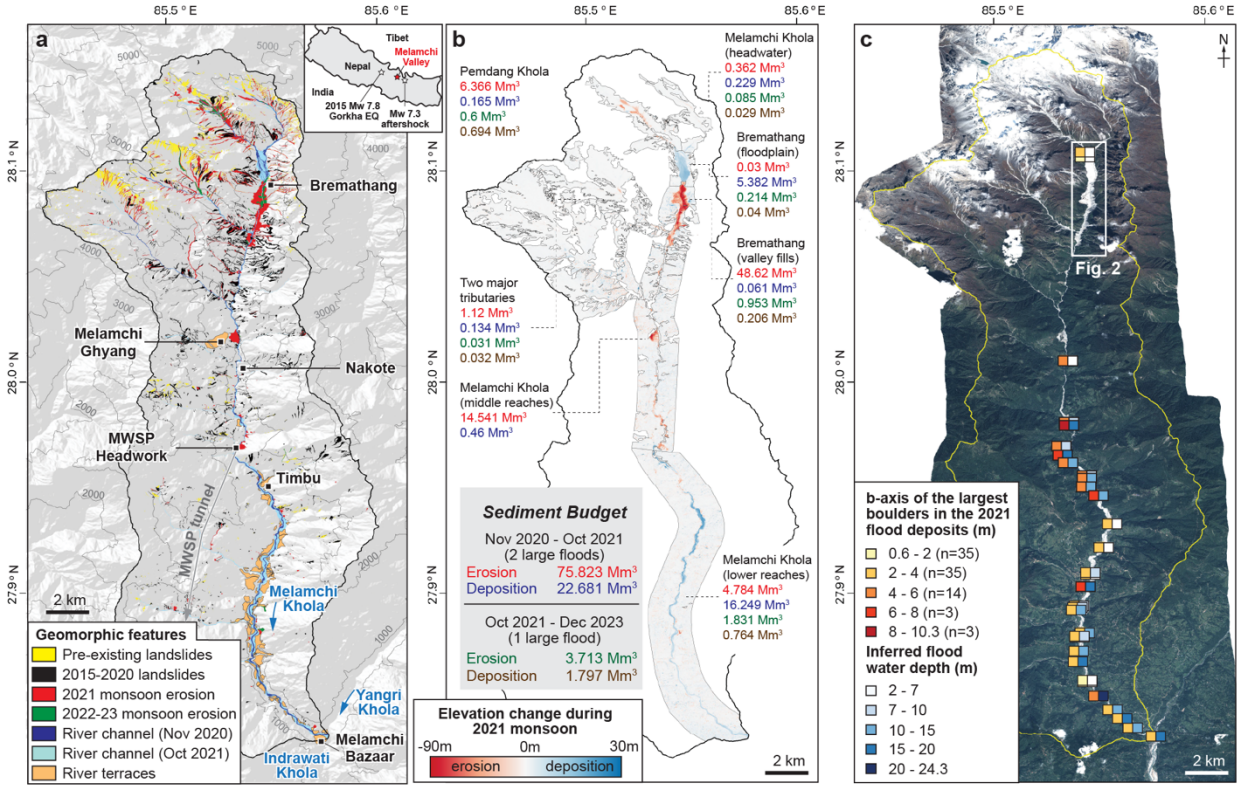

Figure 1. Erosion and deposition patterns of the 2021 Melamchi Flood. (a) Geomorphic features in the Melamchi Valley (total watershed area 324 km^2) include mapped landslides over discrete time intervals (Roback et al. [7]; this study), river channels and terraces. **(b)** Differences of 1 m resolution DSMs quantify the mass transfer from steep Higher Himalaya to gentle Lesser Himalaya during the 2021 flood and subsequent monsoon seasons. **(c)** Field observations and hydraulic reconstruction reveal a high flood stage of 10-20 m in June 2021, resulting in transport of large boulders. Satellite image credit: Pléiades © CNES 2021 and AIRBUS DS.

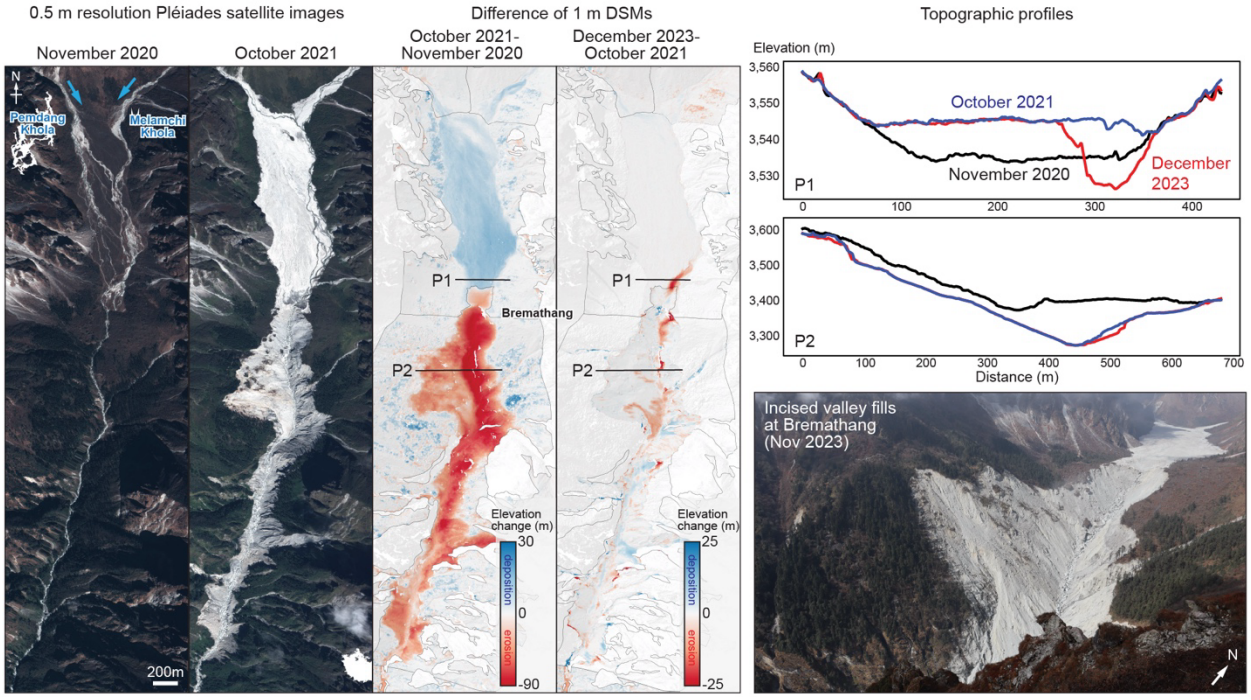

Figure 2. Immense headwater erosion. During the 2021 flood, the valley around Bremathang underwent massive aggradation at its upper floodplain part and intense incision at its lower steep flank, which served as the major sediment source. Satellite image credit: Pléiades © CNES 2020, 2021 and AIRBUS DS.

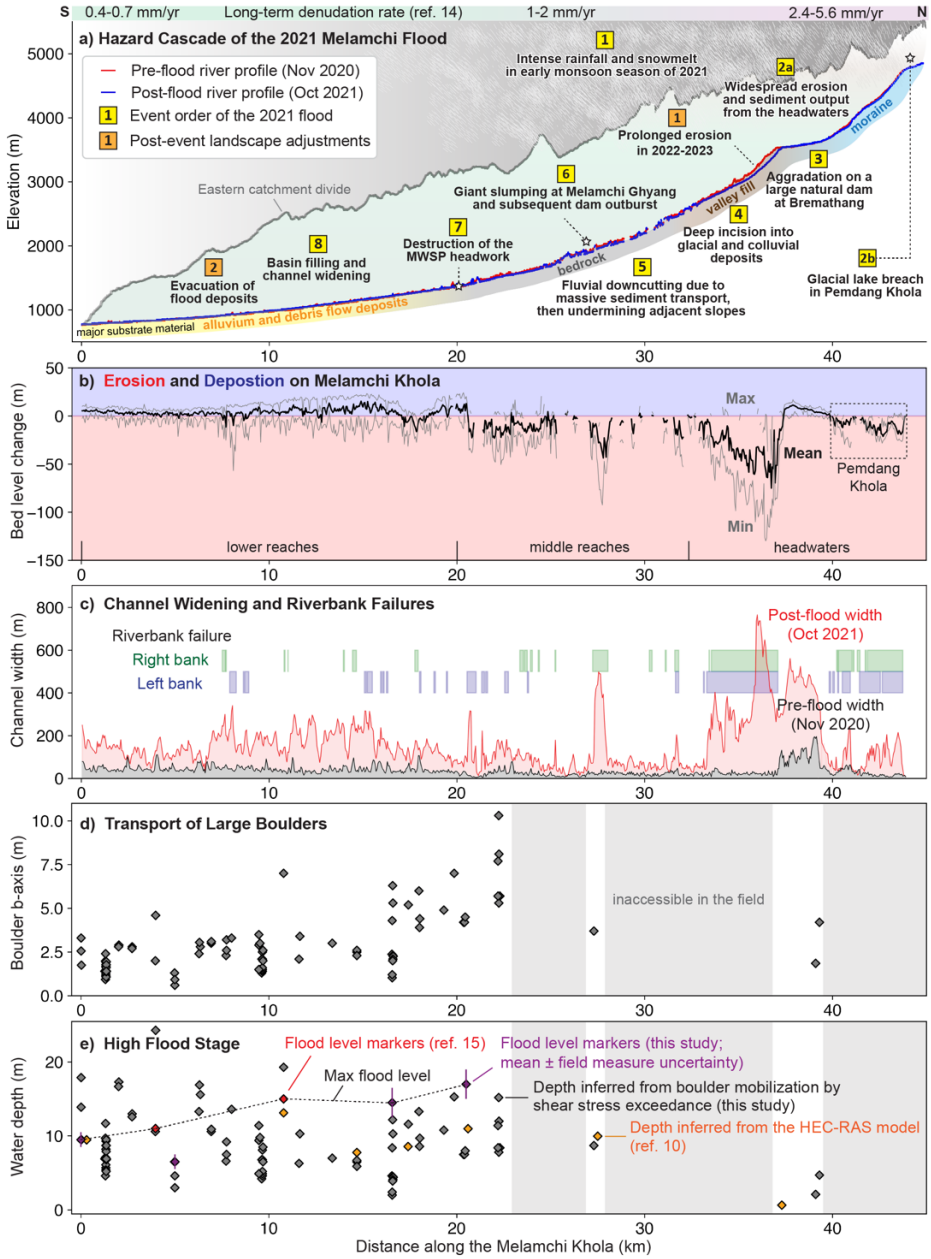

Figure 3. Event Summary. (a) The Melamchi Flood unfolded as a massive "hazard cascade" that involved complex interactions between climate, hydrology, sediment storage, and fluvial processes. This event onset from intense monsoon rainfall and snowmelt that triggered widespread headwater erosion. Then, sediment output from the highest catchments caused a >100 m-deep incision at the large landslide dam at Bremathang. The supply of ~50 Mm^3 of material into the river system fueled debris flooding that undermined slopes downstream, created tens of large bank failures. **(b)** Eventually, the lower reaches were overwhelmed by flood deposits up to 23 m, and **(c)** the main channel was widened two to six times. **(d)** Numerous large boulders (90 measured; b-axis ranging from 0.6 m to 10.3 m) were found in the flood deposits. **(e)** Comparison of boulder sizes with independent constraints on flood hydrologic conditions [10,15] reveals a need of other sediment transport mechanisms besides shear stress exceedance to explain the delivery of boulders in the lowest reaches.

Reference

1 Shugar, D. *et al.* A massive rock and ice avalanche caused the 2021 disaster at Chamoli, Indian Himalaya. *Science* **373**, 300-306 (2021).

2 Cook, K. L., Andermann, C., Gimbert, F., Adhikari, B. R. & Hovius, N. Glacial lake outburst floods as drivers of fluvial erosion in the Himalaya. *Science* **362**, 53-57 (2018).

3 Harrison, S. *et al.* Climate change and the global pattern of moraine-dammed glacial lake outburst floods. *The Cryosphere* **12**, 1195-1209 (2018).

4 Veh, G., Korup, O. & Walz, A. Hazard from Himalayan glacier lake outburst floods. *Proceedings of the National Academy of Sciences* **117**, 907-912 (2020).

5 Cenderelli, D. A. & Wohl, E. E. Flow hydraulics and geomorphic effects of glacial-lake outburst floods in the Mount Everest region, Nepal. *Earth Surface Processes and Landforms: The Journal of the British Geomorphological Research Group* **28**, 385-407 (2003).

6 Rathburn, S. *et al.* The fate of sediment, wood, and organic carbon eroded during an extreme flood, Colorado Front Range, USA. *Geology* **45**, 499-502 (2017).

7 Church, M. & Jakob, M. What is a debris flood? *Water resources research* **56**, e2020WR027144 (2020).

8 Roback, K. *et al.* The size, distribution, and mobility of landslides caused by the 2015 Mw7. 8 Gorkha earthquake, Nepal. *Geomorphology* **301**, 121-138 (2018).

9 Maharjan, S. B. *et al.* The Melamchi flood disaster: Cascading hazard and the need for multihazard risk management. *International Centre for Integrated Mountain Development (ICIMOD), Kathmandu* **10** (2021).

10 Adhikari, T. R. *et al.* Evaluation of post extreme floods in high mountain region: A case study of the Melamchi flood 2021 at the Koshi River Basin in Nepal. *Natural Hazards Research* **3**, 437-446 (2023).

11 Takamatsu, M., Karelia, H. D., Lnu, T. O. & Dahal, R. K. Melamchi Flood Disaster in Nepal: Damage and Risk Quantification with Drone Survey, Satellite-Based Land Displacement Analysis, and 2D Flood Modeling. (2022).

12 Graf, E. L. *et al.* Geomorphological and hydrological controls on sediment export in earthquake-affected catchments in the Nepal Himalaya. *Earth Surface Dynamics* **12**, 135-161 (2024).

13 Jones, J. N., Boulton, S. J., Stokes, M., Bennett, G. L. & Whitworth, M. R. 30-year record of Himalaya mass-wasting reveals landscape perturbations by extreme events. *Nature communications* **12**, 6701 (2021).

14 Medwedeff, W. *Interdependencies between Landslides, Rock Strength, and Landscape Evolution in the Himalaya, Central Nepal*, (2022).

15 Pandey, V. *et al.* Multiperspective field reconnaissance after the melamchi debris flow of June 15, 2021 in central Nepal. *Nepal Engineers' Association (NEA), Lalitpur, Nepal* (2021).

16 Dufek, J. & Bergantz, G. Suspended load and bed-load transport of particle-laden gravity currents: the role of particle–bed interaction. *Theoretical and Computational Fluid Dynamics* **21**, 119-145 (2007).

17 Boyer, C., Roy, A. G. & Best, J. L. Dynamics of a river channel confluence with discordant beds: Flow turbulence, bed load sediment transport, and bed morphology. *Journal of Geophysical Research: Earth Surface* **111** (2006).

18 Todd, S. P. Stream-driven, high-density gravelly traction carpets: possible deposits in the Trabeg Conglomerate Formation, SW Ireland and some theoretical considerations of their origin. *Sedimentology* **36**, 513-530 (1989).

19 Korup, O. & Tweed, F. Ice, moraine, and landslide dams in mountainous terrain. *Quaternary Science Reviews* **26**, 3406-3422 (2007).

20 Schwanghart, W. *et al.* Repeated catastrophic valley infill following medieval earthquakes in the Nepal Himalaya. *Science* **351**, 147-150 (2016).

Methods

Tectonic and climatic context of the Melamchi Valley

The Melamchi Valley is underlain by the Greater Himalaya Crystalline Sequence [1,2] and characterized by a N-S trending exhumation gradient [3-5] controlled by the "flat-ramp" structure of the underlying Main Himalayan Thrust [6,7] (Extended Data Fig. 1). The valley features an orographic rainfall gradient [8]; the mean annual precipitation increases toward the north from ~2 m/yr at Duwachaur (DWC) to 3-4 m/yr at Sermathang (SMT) and Tarkeyghyang (TKG) and then decreases to 1-2 m/yr in the headwaters [9-12] (Extended Data Fig. 1). An automatic weather station in the Upper Melamchi, operated by the International Centre for Integrated Mountain Development (ICIMOD) provides the best evidence about the initiation of the 2021 Melamchi Flood [13]. It reveals that the region had received ~450 mm of rainfall since the monsoon started on May 26, 2021, with two pulses of relatively intense rainfall on May 26-29 and June 11-14 (the maximum hourly rainfall of ~15 mm/hr recorded on June 14). Temperature data from that station and radar images indicate strong snowmelt accompanied with the intense rainfall, indicating that high intensity/duration rainfall, watershed saturation, snowmelt, and potentially rain-on-snow collectively generated the flood on June 15 [13]. Data from rain gauges of the Department of Hydrology and Meteorology (DHM) of the Nepal Government at DWC, SMT, and TKG record considerably lower rainfall during this event, but these sites are far from the flood source area. The June 15 flood unfortunately destroyed the river gauging station on the Melamchi Khola at Nakote. The river stage height record from before the station was damaged is reported in Pandey et al. [14].

Satellite imagery and DSM production

Twelve sets of Pléiades-1A/1B (0.5 m resolution) satellite images were acquired between November 2014 and January 2024 (Supplementary Table 1) to assess the impacts of the 2015 Gorkha Earthquake, 2021 Melamchi Flood, and subsequent 2022-23 monsoon floods on the Melamchi-Indrawati catchment. We mapped the margins of active river channels, which were defined by the absence of vegetation, and then measured their width along the river's central line at a 50 m interval. Landslides and fluvial erosion larger than 3 x 3 pixels were identified. We used the NASA Ames Stereo Pipeline (ASP) software version 3.3.0 [15-17] to construct digital surface models (DSMs) via stereophotogrammetry. To maximize the triangulation accuracy on such a steep terrain, stereo images were first bundle adjusted and map-projected with an external

reference digital terrain model (30 m ALOS DEM) before running *parallel_stereo*. Details of stereo parameterizations are listed in Supplementary Table 2. Point clouds were transformed into 1 m resolution DSMs with outlier filters (*--remove-outliers-params and --max-valid-triangulation-error*).

To quantify flood impacts, we aligned the DSMs before and after the events using a rigid method *Point-to-Plane ICP* (iterative closest point) algorithm with ten iterations to mitigate global misregistration errors (i.e., translation, rotation) and produce the best fitted terrain models. The alignment was based on stable areas only; we selected these areas by excluding any active erosion and deposition visible on satellite imagery, as well as clouds, shadows, ice, and distorted slopes known to deteriorate local DSM quality. Although our stable areas plausibly included small-scale (i.e., less than 1.5 x 1.5 m area) erosion and deposition, extremely small mean (-0.2074 to 0.1299 m for the period of 2020-2021; -0.3955 to 0.0528 m for the period of 2021-2023) and median (-0.0693 to 0.1052 m for 2020-2021; -0.0107 to 0.1377 m for 2021-2023) values of elevation difference on the steady, bedrock-dominated headwater sectors (Supplementary Table 3) suggest that the co-registration performed well, and robust topographic changes can be extracted. In this study, stable areas also include forests and farmlands, which are conventionally regarded as active areas [18,19], but which we included in our alignment in order to enable the calculation of material gain and loss in the forested middle reaches and populated lower segments. Given the timescale of our analysis, we expect changes over these forested and agricultural areas (e.g., due to vegetation change) to be small, justifying their use for alignment in this case.

The uncertainty on a DEM of difference (DoD) can be derived from the error of individual elevation sources [20], if well known, or from direct sampling of elevation difference on stable terrain [19], which also captures potential uncertainty associated with alignment. We sampled the DoD values on stable areas surrounding each active area of interest, calculating the mean, standard deviation (stdev), median, and normalized median absolute deviation (NMAD). We established the level of detection (LoD) at the 95% confidence level using median ± 2 NMAD. We used this approach rather than mean ± 2 standard deviation (stedv) to mitigate the effects of outliers associated with steep slopes. To account for the spatial variation of DSM uncertainty associated with topography, we calculated LoDs for different slope angle ranges (e.g., 0-10, 10-20 degrees).

The statistical results (reported in Extended Data Figs. 2, 3, 5, 7 and Supplementary Table 3) show that gentle slopes (0-20 degrees) have 1/8-1/2th the errors of steep cliffs (60-90 degrees). We also assessed the effect of surface texture and land cover types (i.e., forests, bare rock, and farmland). The results (reported in Extended Data Figs. 2, 3, 5, 7 and Supplementary Table 3) show that the stdev and NMAD of bare rocks are 1-2 times smaller than those of forests. Such observations are consistent with previous findings [18,19]. DoD values below the LoDs were regarded as noisy and eliminated from the budgets of erosion and deposition [20]. Therefore, our results should be interpreted as lower bounds on the topographic change. Our budgets include erosion and deposition of plant material, though their volumetric contribution is quite small, given that most erosion occurred in the rocky headwaters. Our DoD results at eight river sectors are summarized in Figure 1b (see Supplementary Table 3 for detailed data reports).

The DoD results were validated in the field at five locations (Extended Data Figs. 4, 8). We used a tape measure to determine the vertical extent of terrace incision at Sarkathali and flood deposition at Bremathang and Melamchi Bazaar. The coordinates of measuring sites were recorded using a Garmin® handheld GPS receiver with a horizonal accuracy within 5 to 10 meters. The DoD value mean and ranges over the 5 m-radius around the recorded GPS point were then compared with the field measure results. Additionally, we obtained pre- and post-flood photos at the MWSP headworks and at Melamchi Bazaar. The level of aggradation was estimated based on the distance between referenced structures and riverbeds. The vertical accuracy of such photo measures ranged from $\pm$ 1 to $\pm$ 2.5 m.

Boulder size measurement and hydraulic reconstruction

To estimate the transport capacity of the 2021 flood, we measured the size of 90 boulders, targeting the largest observed within accessible reaches of the river (Fig. 1c, 3d, 3e). These measurements were made over three field seasons (Nov 2022, May 2023, Nov 2023). The water depth (h) required for mobilization of these boulder by shear stress exceedance during the flood is estimated by a slope-dependent sediment transport law [21]:

$$\tau = \tau_c(\rho_s - \rho)gd$$

$$\tau_c = 0.15S^{0.25}$$

$$h = \frac{\tau}{\rho g S}$$

where τ_c is the dimensionless critical shear stress depending on channel bed slope (S); ρ_s and ρ are density of sediment (2650 kg/m^3) and water (1000 kg/m^3); g is gravitational acceleration (9.81 m/s^2); and d is the relevant grain size (i.e., boulder b-axis).

In the field, we documented flood level markers at four locations (the MWSP headwork, Timbu, Talamarang, and Melamchi Bazaar; Extended Data Fig. 7) and measured their height (h_1) above the 2021 flood deposits to estimate the true flood water depth (h_t):

$$h_t = h_1 + h_2$$

where h_2 is the deposit thickness derived from DoD. Here we assume instantaneous flood deposition and inundation, but we recognize that riverbed aggradation usually takes place gradually. Thus, h_t should serve as the upper limit for the real flood stage. We compared h and h_t to evaluate sediment transport mechanisms during 2021 flooding (Fig. 3e).

Slope stability analysis

We used the limit equilibrium approach [22] to examine whether the Melamchi Ghyang Landslide could have been caused by rapid downcutting at the toe of the hillslope during flooding (Extended Data Fig. 6). Given the shear-type failure, rocks can be assumed to be Mohr-Coulomb materials in which the shear strength is expressed in cohesion (c) and friction angle (ϕ), and the factor of safety (FoS) can be calculated as follows [23]:

$$FoS = \frac{Resisting forces}{Driving forces} = \frac{cA + W\cos\theta\tan\phi}{W\sin\theta}$$

where A is the area of the sliding plane; W is the weight of the block lying above the sliding plane; θ is the dip angle of the failure plane. Slopes are stable when the resisting forces is greater than the driving forces (FoS>1). Previous Geological Strength Index (GSI) and shallow-geophysics surveys in this region [24] suggested that rock cohesion c is between 0.2 and 1.0 MPa and the friction angle ϕ is between 35° and 40° for hillslope materials. Here we used c = 0.6 MPa and ϕ = 37.5° for the FoS calculation on the Melamchi Ghyang failure. Since the sliding surface geometry of this failure meets the criteria of using the planer sliding model [23], we can evaluate the slope sensitivity to toe cutting in two dimensions. During incision, the failure plane sticks with the slope bottom and A and θ remain constant. Thus, undercutting will add mass into the potential sliding block and increase W, changing the force balance. Pore pressure is not considered here with the aim to

explore the effect of undercutting alone. Pre-incision FoS is >1, while post-incision FoS is <1, indicating change from a stable to unstable slope as a result of the undercutting.

Method-only references

1 Dhital, M.R. (2015). Lesser Himalaya of Bagmati–Gosainkund Region. In: Geology of the Nepal Himalaya. Regional Geology Reviews. Springer, Cham. https://doi.org/10.1007/978-3-319-02496-7_10.

2 Pandey, M., Tandukar, R., Avouac, J., Vergne, J. & Heritier, T. Seismotectonics of the Nepal Himalaya from a local seismic network. *Journal of Asian Earth Sciences* **17**, 703-712 (1999).

3 Robert, X. *et al.* Assessing Quaternary reactivation of the Main Central thrust zone (central Nepal Himalaya): New thermochronologic data and numerical modeling. *Geology* **37**, 731-734 (2009).

4 Herman, F. *et al.* Exhumation, crustal deformation, and thermal structure of the Nepal Himalaya derived from the inversion of thermochronological and thermobarometric data and modeling of the topography. *Journal of Geophysical Research: Solid Earth* **115** (2010).

5 Medwedeff, W. *Interdependencies between Landslides, Rock Strength, and Landscape Evolution in the Himalaya, Central Nepal*, (2022).

6 Pandey, M., Tandukar, R., Avouac, J., Lave, J. & Massot, J. Interseismic strain accumulation on the Himalayan crustal ramp (Nepal). *Geophysical Research Letters* **22**, 751-754 (1995).

7 Hubbard, J. *et al.* Structural segmentation controlled the 2015 Mw 7.8 Gorkha earthquake rupture in Nepal. *Geology* **44**, 639-642 (2016).

8 Bookhagen, B. & Burbank, D. W. Toward a complete Himalayan hydrological budget: Spatiotemporal distribution of snowmelt and rainfall and their impact on river discharge. *Journal of Geophysical Research: Earth Surface* **115** (2010).

9 ICIMOD & UtrechtUniversity. Tipping Bucket: Ganja La 1,2, 3. (2020). https://doi.org: https://doi.org/10.26066/RDS.1972425

10 Steiner, J. F. *et al.* Multi-year observations of the high mountain water cycle in the Langtang catchment, Central Himalaya. *Hydrological Processes* **35**, e14189 (2021).

11 Aryal, A., Maharjan, M., Talchabhadel, R. & Thapa, B. R. Characterizing Meteorological Droughts in Nepal: A Comparative Analysis of Standardized Precipitation Index and Rainfall Anomaly Index. *Earth* **3**, 409-432 (2022).

12 DHM. 2012-2022 daily precipitation at Duwachaur and Sarmathang. (2022).

13 Maharjan, S. B. *et al.* The Melamchi flood disaster: Cascading hazard and the need for multihazard risk management. *International Centre for Integrated Mountain Development (ICIMOD), Kathmandu* **10** (2021).

14 Pandey, V. *et al.* Multiperspective field reconnaissance after the melamchi debris flow of June 15, 2021 in central Nepal. *Nepal Engineers' Association (NEA), Lalitpur, Nepal* (2021).

15 Moratto, Z. M., Broxton, M. J., Beyer, R. A., Lundy, M. & Husmann, K. in *Lunar and Planetary Science Conference.* 2364.

16 Beyer, R. A., Alexandrov, O. & McMichael, S. The Ames Stereo Pipeline: NASA's open source software for deriving and processing terrain data. *Earth and Space Science* **5**, 537-548 (2018).

17 Broxton, M. J. & Edwards, L. J. in *39th Annual Lunar and Planetary Science Conference.* 2419.

18 Nuth, C. & Kääb, A. Co-registration and bias corrections of satellite elevation data sets for quantifying glacier thickness change. *The Cryosphere* **5**, 271-290 (2011).

19 Hugonnet, R. *et al.* Uncertainty analysis of digital elevation models by spatial inference from stable terrain. *IEEE Journal of Selected Topics in Applied Earth Observations and Remote Sensing* **15**, 6456-6472 (2022).

20 Lane, S. N., Westaway, R. M. & Murray Hicks, D. Estimation of erosion and deposition volumes in a large, gravel-bed, braided river using synoptic remote sensing. *Earth surface processes and landforms: the journal of the British Geomorphological Research Group* **28**, 249-271 (2003).

21 Lamb, M. P., Dietrich, W. E. & Venditti, J. G. Is the critical Shields stress for incipient sediment motion dependent on channel-bed slope? *Journal of Geophysical Research: Earth Surface* **113** (2008).

22 Azarafza, M. *et al.* Discontinuous rock slope stability analysis by limit equilibrium approaches–a review. *International Journal of Digital Earth* **14**, 1918-1941 (2021).

23 Wyllie, D. C. & Mah, C. *Rock slope engineering*. (CRC Press, 2004).

24 Medwedeff, W. G., Clark, M. K., Zekkos, D., West, A. J. & Chamlagain, D. Near-surface geomechanical properties and weathering characteristics across a tectonic and climatic gradient in the Central Nepal Himalaya. *Journal of Geophysical Research: Earth Surface* **127**, e2021JF006240 (2022).

Data Availability

Geomorphologic mapping data are available in HydroShare (doi: 10.4211/hs.b6da096000284d5882d13b085b7669ac). Source data are provided with this paper. DSM data are available in Open-Topography (https://doi.org/10.5069/G9R78CFK).

Ethics & Inclusion statement

Fieldwork that contributed to this study included several Nepali researchers and local community members and was approved by relevant government agencies. We have cited reports related to the 2021 flood that we are aware of, and we acknowledge their important contributions to understanding this event and its impacts. The research forms part of a body of knowledge on geohazards in the central Nepal that we hope can contribute to preparedness and to future sustainability of local communities and infrastructure including the Melamchi Water Supply Project.

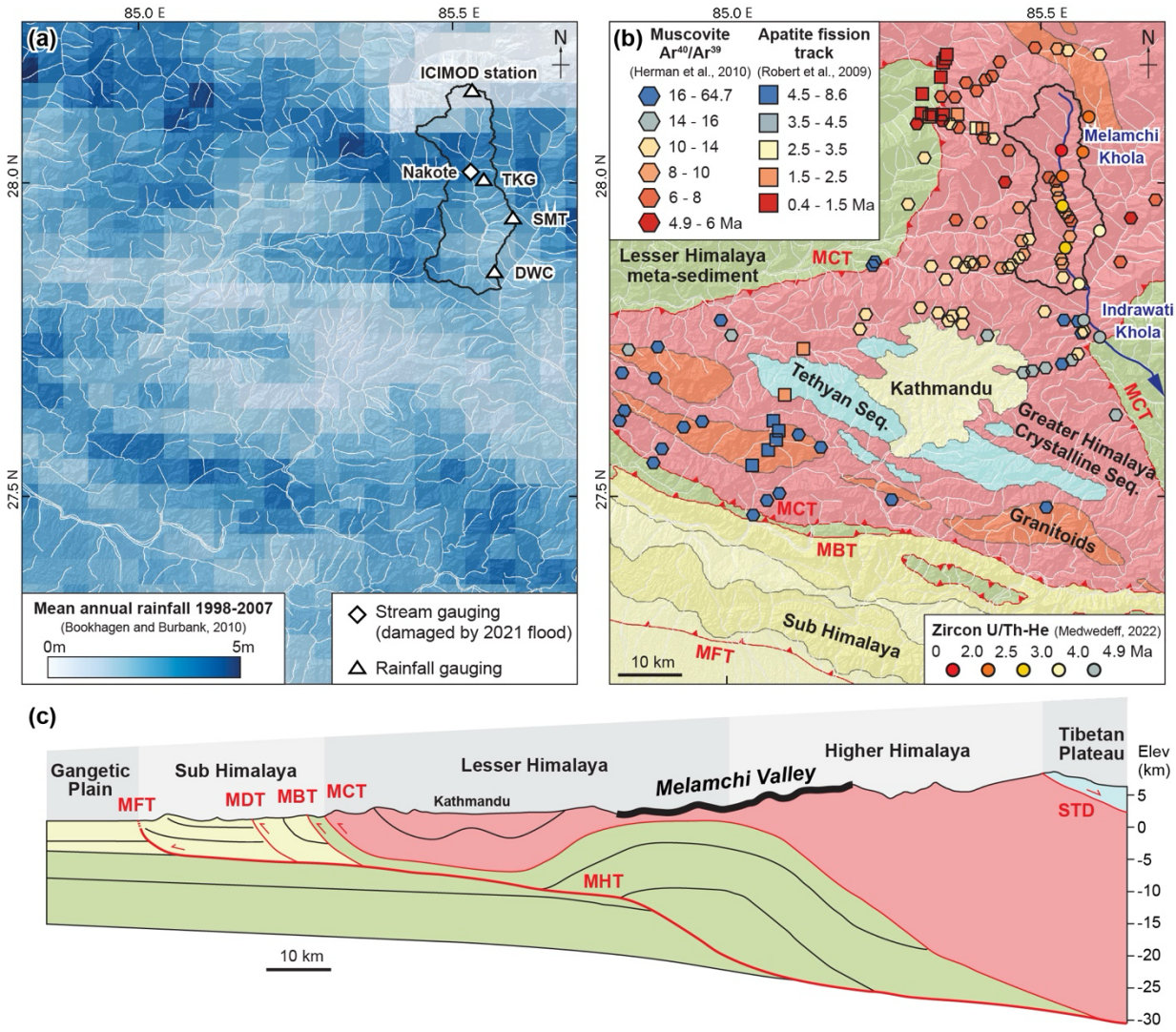

Extended Data Fig. 1. Context of the Melamchi Valley. The Melamchi valley features N-S gradients of (a) orographic rainfall (Bookhagen & Burbank, 2010) and (b) exhumation rate (Robert et al., 2009; Herman et al. 2010; Medwedeff, 2022). Geologic map modified from Dhital (2015). The major faults in the orogenic system include the Main Himalayan Thrust (MHT), Main Frontal Fault (MFT), Main Boundary Thrust (MBT), Main Central Thrust (MCT), and South Tibetan Detachment (STD). (c) Geologic Profile under Kathmandu-Melamchi Valley. Modified from Pandey et al. (1995).

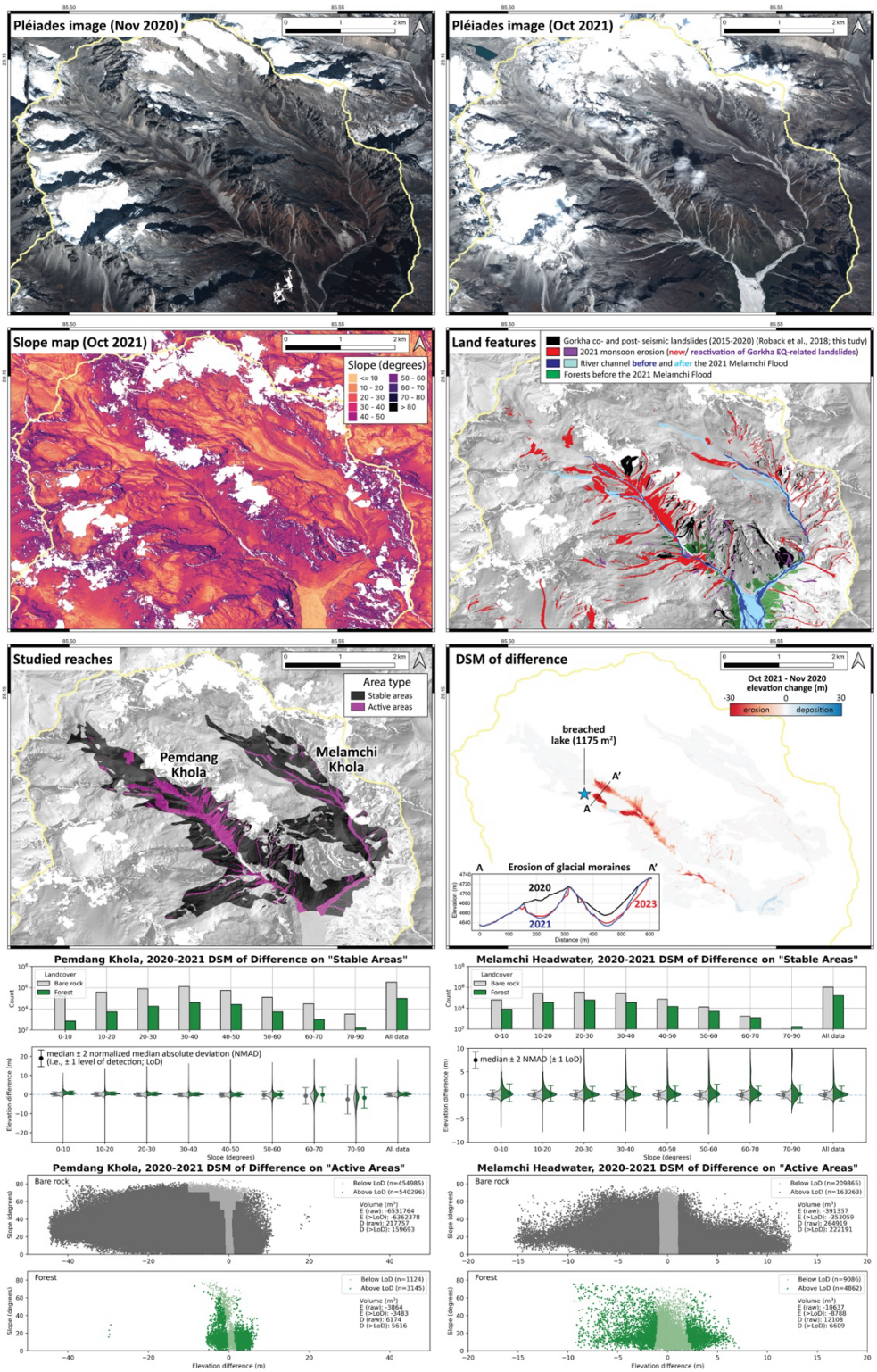

Extended Data Fig. 2. Geomorphic impacts of the 2021 flood in the Melamchi headwaters. Massive sediment outputs were observed after the flood, especially in the Pemdang Khola where glacial moraines were cut by up to 40 m. Some 2021 activity was associated with landslides from the 2015 Gorkha earthquake, but most erosion was new. Satellite image credit: Pléiades © CNES 2020, 2021 and AIRBUS DS.

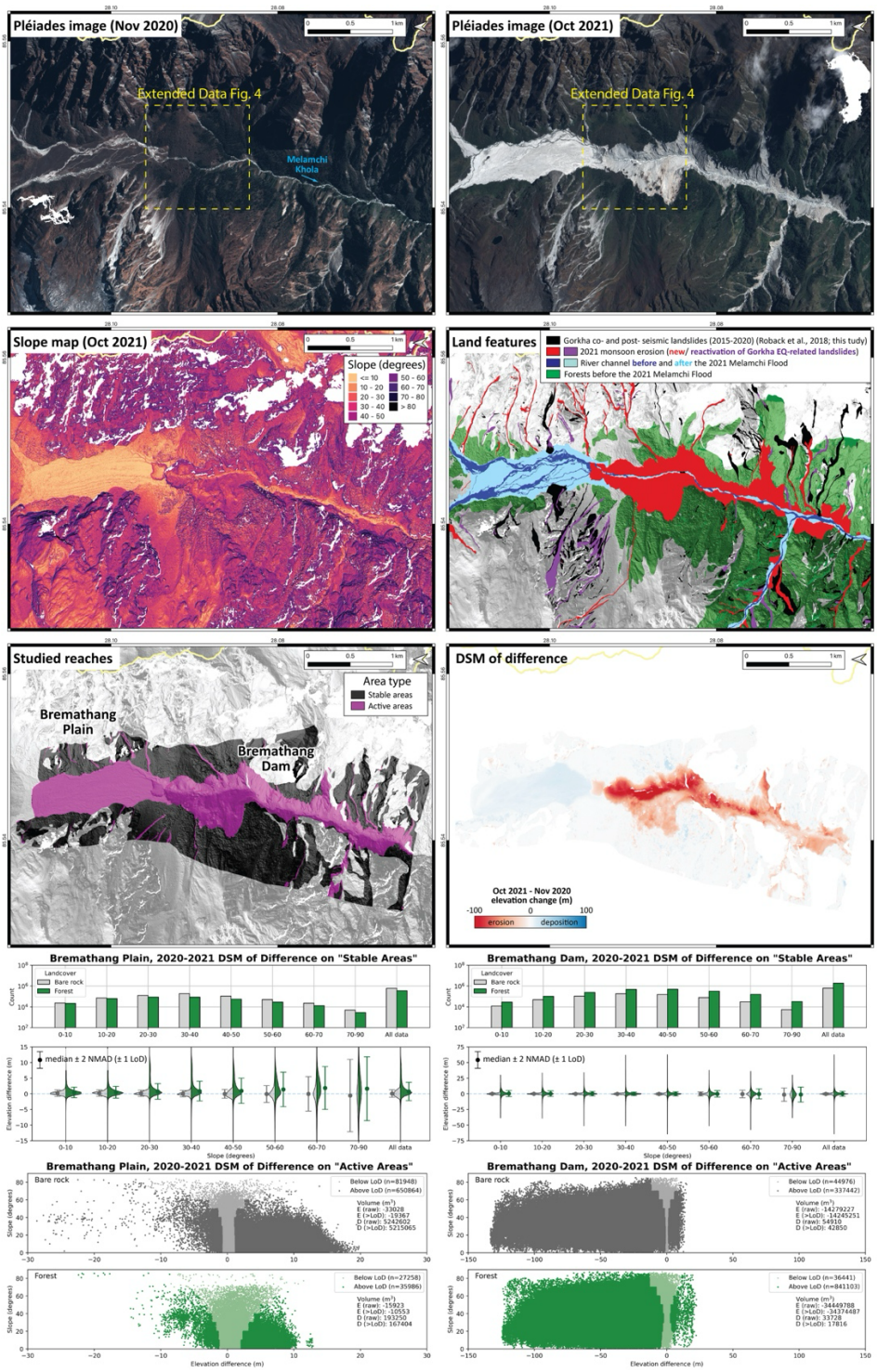

Extended Data Fig. 3. Geomorphic impacts of the 2021 flood around Bremathang. The top of the large landslide dam was covered by 5-10 m of flood deposits, while its lower, steep part experienced >100 m incision.

Satellite image credit: Pléiades © CNES 2020, 2021 and AIRBUS DS.

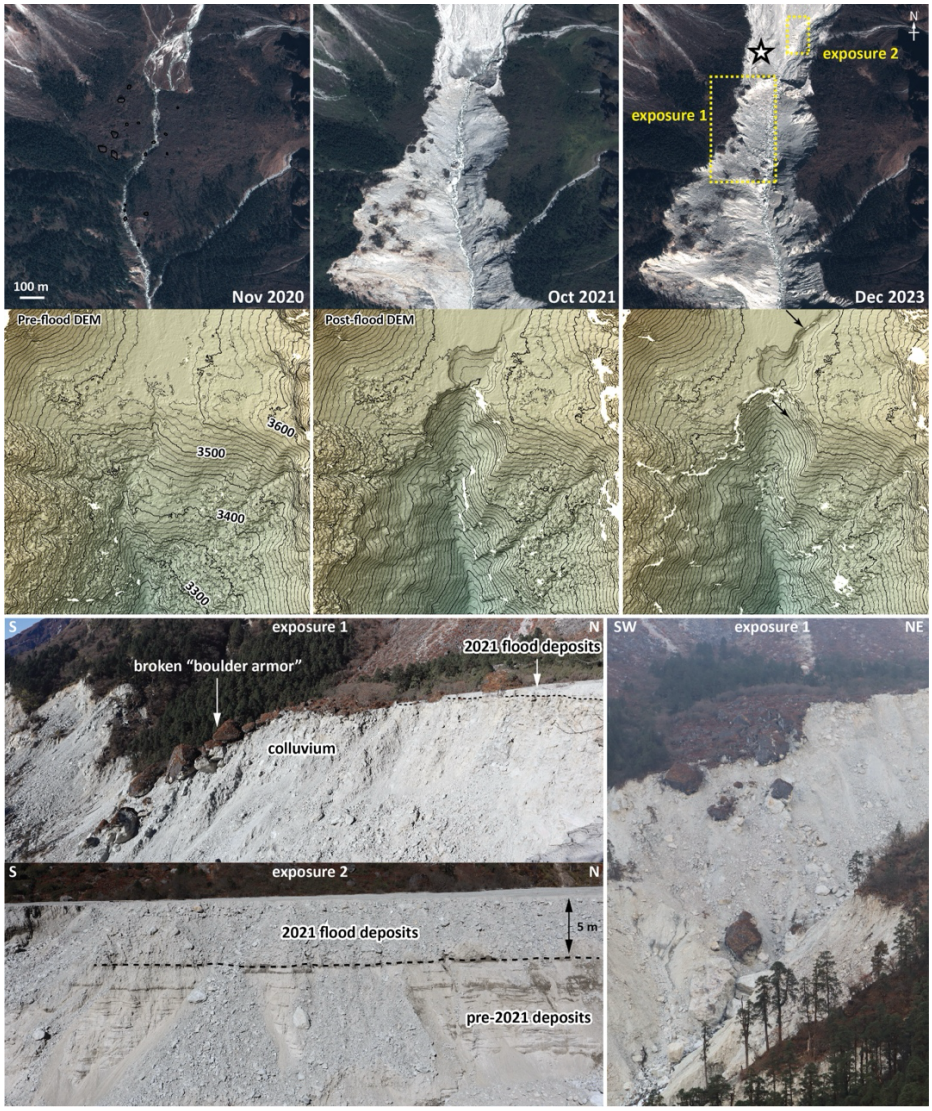

Extended Data Fig. 4. Observations of the Bremathang Dam incision. Top: Geometry of the Bremathang natural dam before and after the 2021 and 2023 floods. Topographic and sedimentary evidence suggests that the dam had been stable for a long period before the floods. No active erosion was observed on the dam surface before 2021. Arrows on contour maps from 2023 show new erosional activity since 2021, most occurring in August 2023 (also see Fig. 1). Bottom: The profiles of the sediment deposits behind the dam, exposed by erosion during the 2021 flood, reveal (1) remnants of a carpet of giant boulders that protected the dam and (2) a thick layer (at least 10 m) of fine-grained material (predominantly sand size fraction from field observations) beneath coarser deposits that we attribute to the 2021 flood. Deposit thickness is between 5.074 and 5.29 m indicated from DoD, validated by field measurement (5.181 m) at the star-marked site in May 2024. The origin of the dam is unclear but plausibly related to past glacial advances and mass-wasting processes on surrounding steep slopes.

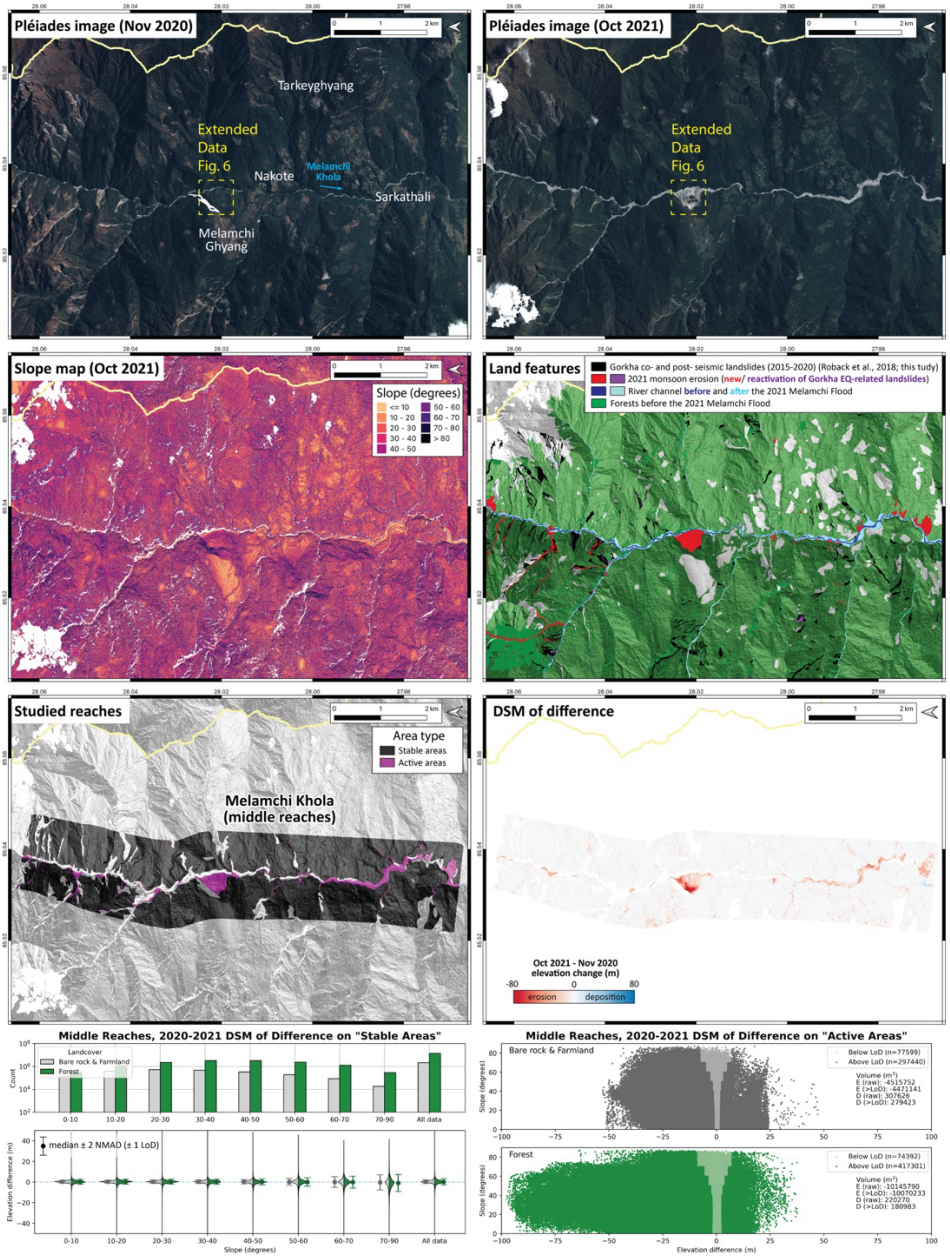

Extended Data Fig. 5. Geomorphic impacts of the 2021 flood in the middle reaches of Melamchi Khola. Slope failures and riverbed downcutting occurred due to intensive sediment transport. Satellite image credit: Pléiades © CNES 2020, 2021 and AIRBUS DS.

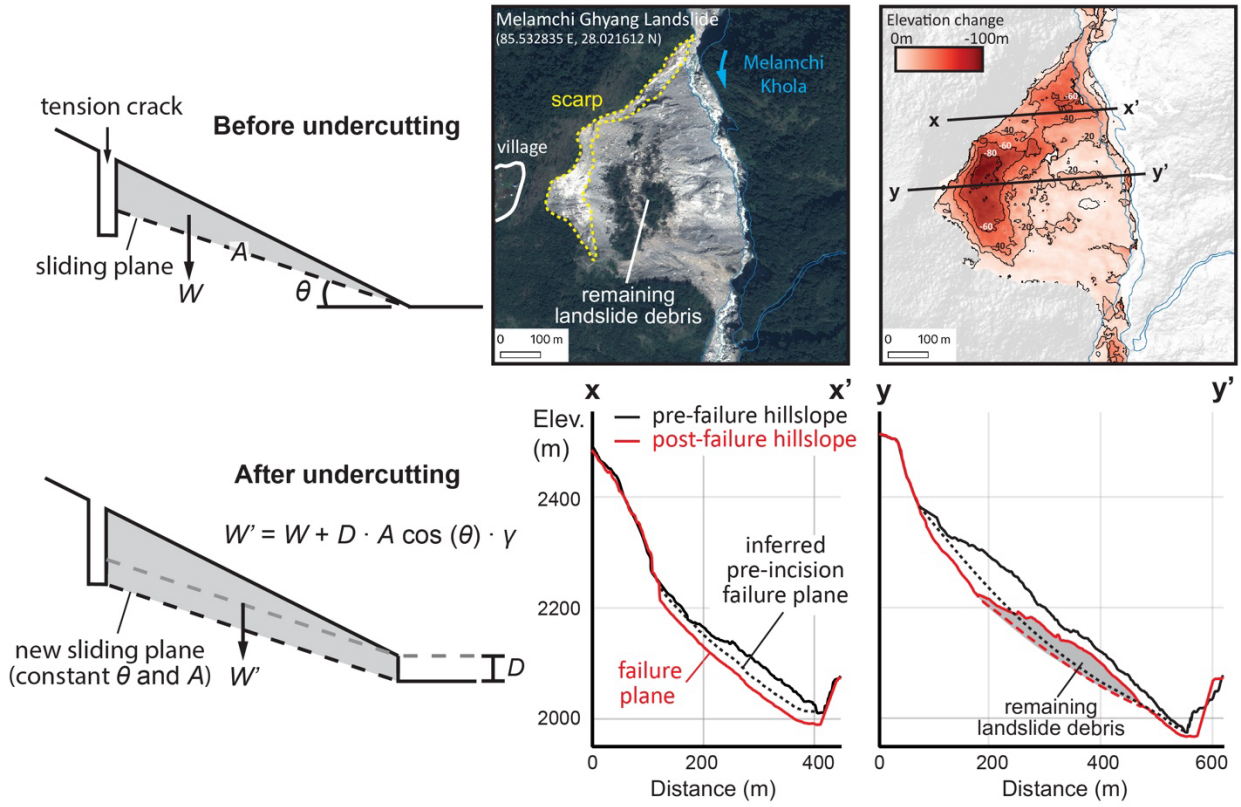

		Profile x-x'	Profile y-y'
Assuming a dry condition	incision depth (D) =	21 m	15 m
rock unit weight (γ) = 26.5 kN/m³	failure plane angle (θ) =	42 ± 3°	40 ± 4°
rock cohesion (c) = 0.6 MPa *	sliding plane area (A) =	370 ± 20 m²/m	650 ± 50 m²/m
rock friction angle (ϕ) = 37.5° *	**pre-incision**		
* Medwedeff et al. (2022)	block weight (W) =	147,075 ± 7,950 kN/m	396,175 ± 30,475 kN/m
	factor of safety (FoS) =	**1.392** (+0.059/-0.067)	**1.011** (+0.056/-0.067)
	post-incision		
	block weight (W') =	300,092 ± 16,221 kN/m	634,258 ± 48,789 kN/m
	factor of safety (FoS') =	**0.877** (+0.043/-0.047)	**0.691** (+0.053/-0.062)

Extended Data Fig. 6. Slope stability analysis for the toe-cutting scenario at the Melamchi Ghyang Landslide. We used the limit equilibrium approach (Azarafza et al., 2021) with the planer sliding model (Wyllie & Mah, 2004) to examine the cause of the Melamchi Ghyang Landslide. We found that the factor of safety (FoS) dropped under 1 after 15-21 m incision, supporting the hypothesis of rapid downcutting at the toe of the hillslope during flooding. Satellite image credit: Pléiades © CNES 2021 and AIRBUS DS.

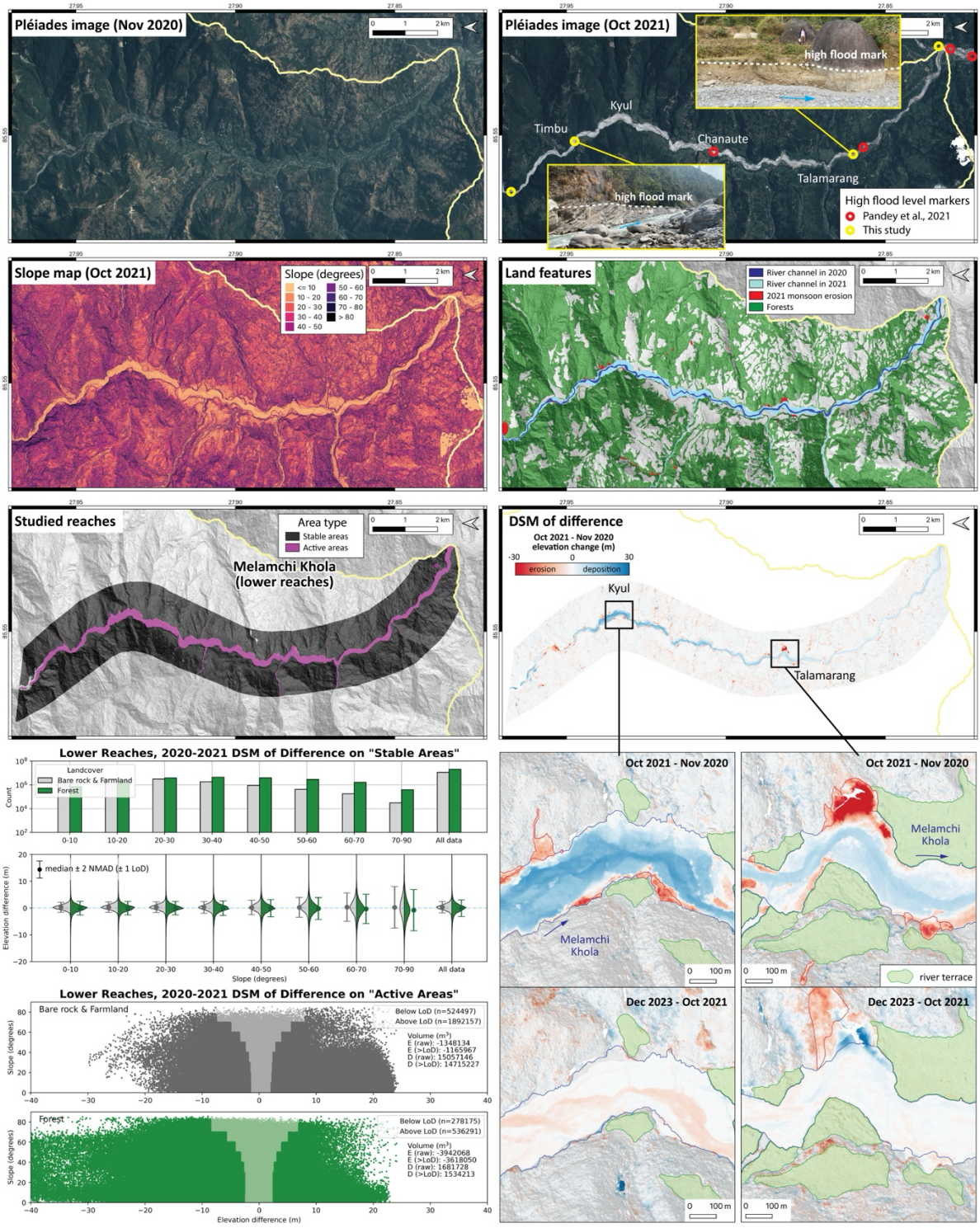

Extended Data Fig. 7. Geomorphic impacts of the 2021 flood in the lower reaches of Melamchi Khola. Massive aggradation (15-23 m) was observed on the riverbed near Kyul. Following change detection indicates rapid evacuation of sediment (1-6 m lowering between Oct 2021 and Dec 2023). Intense lateral erosion and large slope failure at where the river curves near Talamarang. The slope failure extended further upslope during Oct 2021-Dec 2023. Satellite image credit: Pléiades © CNES 2020, 2021 and AIRBUS DS.

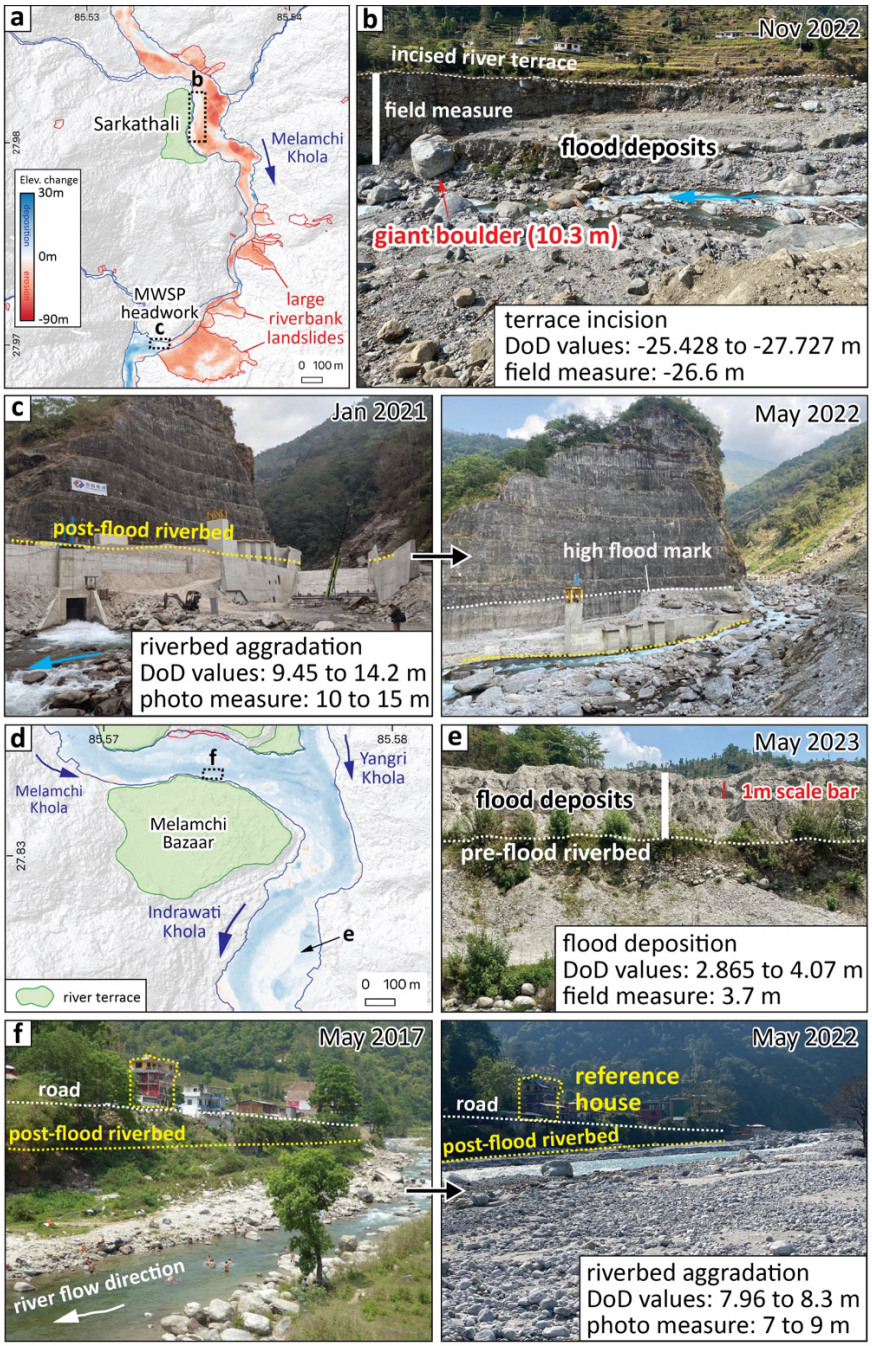

Extended Data Fig. 8. Field observations in the middle and lower reaches of the Melamchi Khola. The DoD results were validated at Sarkathali, the MWSP headwork, and Melamchi Bazaar. Elevation change measurements are consistent between the DoD and in-situ observations. (a-c) Incision of terrace and debris fan deposits around Sarkathali, large riverbank landslides between Sarkathali and the headwork of the Melamchi Water Supply Project (MWSP), and significant aggradation around and below the headwork site. (d-f) Aggradation of 5-10 m around the confluence of the Melamchi Khola and Yangri Khola. Contrast to the upstream parts, post-flood sediment evacuation around and below this area has been significantly contributed by anthropogenic activities, such as gravel mining and river engineering, according to our field observations and interviews.

Table S1. Stereo satellite imagery used in this study.					
Pair	**Spatial extent**	**Satellite**	**File name**	**Acquisition time**	**Cloud cover**
1	N028°03'32" - N028°16'51", E085°26'44" - E085°36'27"	Pléiades 1A	5906795101	11/9/14 5:03	0%
		Pléiades 1B	5906796101	11/1/14 5:15	3.35%
2	N027°49'36" - N028°00'15", E085°28'32" - E085°37'05"	Pléiades 1A	5906797101	12/5/14 5:04	0.39%
		Pléiades 1B	5906798101	11/29/14 5:00	0.25%
3	N027°58'10" - N028°10'11", E085°28'35" - E085°35'39"	Pléiades 1A	5906792101	11/13/20 5:11	0%
		Pléiades 1B	5906791101	11/19/20 5:15	0%
4	N028°01'17" - N028°09'29", E085°22'50" - E085°30'00"	Pléiades 1A	5906794101	11/13/20 5:11	0%
		Pléiades 1B	5906793101	11/19/20 5:15	0%
5	N027°42'33" - N027°59'37", E085°29'40" - E085°37'40"	Pléiades 1A	5906800101	1/11/21 5:07	0%
		Pléiades 1A	5906799101	1/18/21 5:04	1.31%
6	N027°42'23" - N027°51'37", E085°26'21" - E085°37'34"	Pléiades 1B	6004961101	10/11/21 5:08	4.55%
		Pléiades 1B	6004962101	10/11/21 5:08	5.44%
7	N027°49'54" - N028°10'52", E085°25'37" - E085°37'31"	Pléiades 1A	6005840101	10/12/21 5:00	1.26%
		Pléiades 1A	6005841101	10/12/21 5:01	1.85%
8	N027°59'12" - N028°10'23", E085°26'08" - E085°35'26"	Pléiades 1B	6890961101	12/19/23 5:11	0%
		Pléiades 1B	6890962101	12/19/23 5:11	0%
9	N027°36'24" - N027°48'00", E085°35'47" - E085°40'31"	Pléiades 1B	6893039101	12/26/23 5:07	0%
		Pléiades 1B	6893040101	12/26/23 5:08	0%
10	N027°25'02" - N027°47'05", E085°38'47" - E085°51'05"	Pléiades 1B	6893041101	12/26/23 5:07	0.27%
		Pléiades 1B	6893042101	12/26/23 5:08	0.19%
11	N027°42'32" - N027°51'29", E085°26'21" - E085°37'36"	Pléiades 1B	6893043101	12/26/23 5:07	0%
		Pléiades 1B	6893044101	12/26/23 5:07	0%
12	N027°49'24" - N028°01'26", E085°26'26" - E085°37'18"	Pléiades 1B	6902874101	1/9/24 4:59	2.04%
		Pléiades 1B	6902875101	1/9/24 5:00	2.63%

Table S2. Parameters invoked in the NASA Ames Stereo Pipeline algorithm for DSM production.		
Tool	**Parameter**	**Value**
bundle_adjust	--ip-per-image	10000
	--tri-weight	0.1
	--tri-robust-threshold	0.1
	--camera-weight	0
parallel_stereo	--stereo-algorithm	asp_final_mgm
	--cost-mode	3
	--xcorr-threshold	-1
	--min-xcorr-level	1
	--subpixel-mode	12
	--corr-kernel	9 9
	--corr-tile-size	2048
	--sgm-collar-size	512
	--corr-memory-limit-mb	4096
	--filter mode	2
	--rm-threshold	3.5
	--rm-min-matches	50
	--rm-half-kernel	9 9
	--rm-cleanup-passes	1
	--max-disp-spread	100
	--ip-per-image	10000
	--num-matches-from-disparity	90000
point2dem	--median-filter-params	9 9
	--remove-outliers-params	95 3
	--max-valid-triangulation-error	2
	--erode-length	0
pc_align	--alignment-method	Point-to-Plane ICP
	--max-displacement	50
	--num-iterations	10
	--highest-accuracy	

Uncertainty analysis of DSMs of difference (Oct 2021- Nov 2020) on defined stable areas

Reach	Landcover	Sample number/ Sample area	Statistics of DSM of difference	Slope (degrees)								
				0-10	10-20	20-30	30-40	40-50	50-60	60-70	70-90	All
Melamchi Khola (headwater)	bare rock	1041849	Mean	0.1656	0.1475	0.1306	0.1185	0.0909	0.0647	-0.0934	-0.054	0.1299
			Stdev	0.6378	0.6454	0.6536	0.6283	0.6509	0.7228	0.6699	0.5489	0.645
			Median	0.1291	0.1145	0.1052	0.1023	0.0732	0.0496	-0.0714	-0.12	0.1052
			NMAD	0.5107	0.4955	0.5039	0.4963	0.5223	0.5328	0.5288	0.3898	0.5017
			LoD	1.0214	0.991	1.0077	0.9926	1.0445	1.0656	1.0576	0.7795	1.0034
	forest	159998	Mean	1.1662	0.9476	0.8259	0.7675	0.8921	1.2452	1.77	3.6683	0.8871
			Stdev	1.8908	1.7154	1.6416	1.5588	1.7176	2.2188	2.9682	3.7757	1.7082
			Median	0.5328	0.4269	0.3508	0.3403	0.4241	0.5981	0.8801	2.1655	0.3857
			NMAD	0.9275	0.7875	0.7294	0.7294	0.8691	1.2419	1.858	3.2432	0.7789
			LoD	1.855	1.575	1.4587	1.4589	1.7382	2.4837	3.716	6.4864	1.5578
Pemdang Khola	bare rock	3302377	Mean	0.2619	0.1292	-0.0075	-0.0924	-0.2374	-0.5478	-1.0289	-2.9979	-0.0816
			Stdev	0.8366	0.8264	0.8671	1.0061	1.522	2.5613	3.6643	4.6263	1.2213
			Median	0.2292	0.1094	-0.0066	-0.0525	-0.1133	-0.2378	-0.6826	-2.4996	-0.0261
			NMAD	0.5911	0.5809	0.5256	0.5143	0.6063	1.0247	2.1754	3.8297	0.5621
			LoD	1.1822	1.1618	1.0511	1.0285	1.2126	2.0494	4.3507	7.6594	1.1242
	forest	93823	Mean	0.9987	0.7429	0.4995	0.2484	0.111	0.0022	0.0155	-1.8947	0.2712
			Stdev	1.0046	0.9553	0.9569	0.8156	0.9706	1.4506	2.3944	2.5384	0.9978
			Median	0.8379	0.5576	0.3373	0.1638	0.0418	-0.0442	-0.0457	-1.6853	0.1909
			NMAD	0.5151	0.4742	0.4859	0.4905	0.59	0.9509	1.9354	2.6669	0.5589
			LoD	1.0302	0.9484	0.9718	0.9811	1.18	1.9018	3.8707	5.3337	1.1177
Brematang Plain	bare rock	595807	Mean	0.2828	0.2568	0.177	-0.0073	-0.1931	-0.3678	-0.2088	-1.1418	-0.0061
			Stdev	1.0353	1.2517	1.5375	1.9357	2.783	3.8866	4.985	7.875	2.4681
			Median	0.2158	0.2168	0.1816	0.0684	-0.0186	-0.0664	-0.02	-0.5527	0.1025
			NMAD	0.514	0.5082	0.4995	0.5227	0.6993	1.3595	2.7661	5.7943	0.6095
			LoD	1.028	1.0164	0.9991	1.0454	1.3986	2.7191	5.5322	11.5886	1.2189
	forest	355948	Mean	1.0789	1.3053	1.7361	1.838	1.8369	1.9006	2.0361	2.23	1.689
			Stdev	2.4741	2.7388	3.1436	3.5621	3.6956	4.1088	4.7976	6.58	3.444
			Median	0.4277	0.498	0.7578	0.8647	0.9746	1.4014	1.8647	1.6416	0.7568
			NMAD	0.834	0.9397	1.2524	1.5861	2.0154	2.7625	3.4227	5.1037	1.4667
			LoD	1.668	1.8794	2.5047	3.1722	4.0307	5.525	6.8453	10.2074	2.9334
Brematang Dam	bare rock	624926	Mean	0.3164	0.2082	0.0493	-0.1151	-0.2953	-0.4848	-0.5821	-1.6319	-0.1811
			Stdev	2.5807	2.6466	2.7322	2.709	3.1705	4.4771	5.5111	6.4777	3.333
			Median	0.0732	0.0469	-0.0098	-0.0488	-0.1455	-0.2402	-0.2705	-1.2861	-0.0693
			NMAD	0.7471	0.6602	0.6515	0.737	0.9092	1.6071	3.0883	5.331	0.8731
			LoD	1.4942	1.3204	1.303	1.474	1.8183	3.2141	6.1766	10.662	1.7461
	forest	1866290	Mean	0.6849	0.5639	0.3131	0.0299	-0.1452	-0.3313	-0.5986	-1.4644	-0.0809
			Stdev	5.0093	4.8495	4.5966	4.2073	4.4509	5.2773	6.0126	7.1402	4.8127
			Median	0.3955	0.3203	0.1846	0.0566	-0.0215	-0.0586	-0.2207	-1.1943	0.04
			NMAD	2.4266	2.1949	1.7606	1.3566	1.665	2.6293	3.9787	5.9883	1.9561
			LoD	4.8531	4.3897	3.5212	2.7132	3.33	5.2585	7.9573	11.9766	3.9122

Reach	Landcover	Sample number/ Sample area	Statistics of DSM of difference	Slope (degrees)								
				0-10	10-20	20-30	30-40	40-50	50-60	60-70	70-90	All
Helambu Khola	bare rock	6582968	Mean	0.067	0.0179	-0.0196	-0.075	-0.1659	-0.3761	-0.7352	-1.3549	-0.0714
			Stdev	0.9758	0.8255	0.7136	0.8366	1.3011	2.1319	2.9859	4.6607	1.0312
			Median	0.0791	0.0137	-0.0254	-0.0791	-0.1328	-0.2266	-0.5029	-1.3144	-0.0488
			NMAD	0.5227	0.501	0.4923	0.5169	0.6732	1.083	1.8996	3.5436	0.5444
			LoD	1.0454	1.002	0.9845	1.0338	1.3463	2.166	3.7993	7.0873	1.0888
	forest	699806	Mean	0.5956	0.3089	0.1656	-0.0282	-0.1233	-0.1735	-0.3483	-1.2733	-0.0729
			Stdev	2.1585	1.8203	1.7512	1.8027	2.2178	2.9551	3.9003	5.5773	2.4258
			Median	0.1211	-0.03	-0.0596	-0.1045	-0.1523	-0.1582	-0.2822	-0.856	-0.1133
			NMAD	0.8028	0.6168	0.6646	0.6834	0.8644	1.4811	2.5482	4.1003	0.8687
			LoD	1.6057	1.2336	1.3293	1.3668	1.7287	2.9622	5.0964	8.2006	1.7373
Namsang Khola	bare rock	15739619	Mean	-0.066	-0.085	-0.0802	-0.1465	-0.3436	-0.8872	-1.7894	-2.9667	-0.2074
			Stdev	1.3674	1.1692	1.1088	1.3131	2.015	3.3206	4.322	5.0917	1.6414
			Median	-0.024	-0.053	-0.0478	-0.0879	-0.1748	-0.373	-1.0625	-2.4771	-0.0869
			NMAD	0.6515	0.6153	0.6168	0.6544	0.7934	1.2669	2.2224	3.6725	0.6776
			LoD	1.303	1.2306	1.2335	1.3087	1.5868	2.5338	4.4448	7.345	1.3551
	forest	6786899	Mean	-0.31	-0.271	-0.205	-0.2047	-0.4117	-0.76	-1.2619	-2.3375	-0.4768
			Stdev	3.4626	3.4172	3.3016	3.2964	3.8816	4.5942	5.3369	6.3351	3.9683
			Median	-0.007	-0.002	0.0459	0.0635	-0.043	-0.2871	-0.6914	-1.4736	-0.0166
			NMAD	0.9585	0.9889	0.9918	0.9961	1.3972	2.3209	3.5038	4.7229	1.3711
			LoD	1.917	1.9777	1.9836	1.9923	2.7944	4.6418	7.0075	9.4457	2.7422
Melamchi Khola (middle reaches)	bare rock & farmland	2103667	Mean	0.2556	0.2727	0.2391	0.123	-0.0766	-0.2581	-0.5244	-1.233	0.0844
			Stdev	1.2133	1.2793	1.5239	2.0829	2.8206	3.6386	4.5178	5.5192	2.3357
			Median	0.2891	0.3242	0.3203	0.2773	0.1973	0.0977	0	-0.3618	0.2705
			NMAD	0.7514	0.7688	0.8398	0.9237	1.1105	1.6621	2.5902	3.6746	0.9527
			LoD	1.5028	1.5376	1.6795	1.8473	2.221	3.3242	5.1803	7.3492	1.9055
	forest	13943123	Mean	-0.026	-0.03	-0.0434	-0.0529	-0.1221	-0.2462	-0.5058	-1.5595	-0.1706
			Stdev	2.9214	2.8441	2.8198	2.8538	3.1395	3.67	4.351	5.65	3.3101
			Median	0.2412	0.2363	0.2246	0.209	0.1494	0.0254	-0.1514	-0.9971	0.1465
			NMAD	1.2379	1.1959	1.1713	1.2133	1.4623	2.0284	2.8754	4.1293	1.5043
			LoD	2.4758	2.3917	2.3425	2.4266	2.9246	4.0567	5.7508	8.2586	3.0085
Melamchi Khola (lower reaches)	bare rock & farmland	11182307	Mean	0.3069	0.3655	0.3402	0.2275	0.162	0.1994	0.2977	0.3421	0.3052
			Stdev	1.1904	1.253	1.3644	1.6436	2.1451	2.8309	3.5591	4.5298	1.6095
			Median	0.2861	0.3516	0.3447	0.2588	0.2197	0.2529	0.333	0.2744	0.3125
			NMAD	0.9324	0.973	1.0092	1.1033	1.3537	1.8648	2.6568	3.8773	1.0584
			LoD	1.8647	1.946	2.0184	2.2065	2.7074	3.7296	5.3135	7.7546	2.1167
	forest	20172660	Mean	-0.299	-0.276	-0.2565	-0.2543	-0.2773	-0.3376	-0.4394	-0.7304	-0.2956
			Stdev	2.5386	2.5048	2.4901	2.6074	2.8923	3.3112	3.7994	4.8348	2.9449
			Median	-0.063	-0.056	-0.0508	-0.0557	-0.084	-0.1543	-0.3144	-0.791	-0.0791
			NMAD	1.2886	1.2741	1.2727	1.3624	1.6115	2.0545	2.7364	3.8571	1.568
			LoD	2.5771	2.5482	2.5454	2.7248	3.2231	4.1089	5.4728	7.7143	3.136

Uncertainty analysis of DSMs of difference (Dec 2023- Oct 2021) on defined stable areas

Reach	Landcover	Sample number/ Sample area	Statistics of DSM of difference	Slope (degrees)								
				0-10	10-20	20-30	30-40	40-50	50-60	60-70	70-90	All
Melamchi Khola (headwater)	bare rock	2567805	Mean	-0.0269	-0.0282	-0.0055	0.0081	0.0128	-0.0234	-0.1803	-0.2452	-0.0061
			Stdev	0.3946	0.4002	0.4386	0.4871	0.6447	1.0375	1.801	3.3996	0.4901
			Median	-0.0283	-0.0322	-0.0107	0.0078	0.0117	-0.0283	-0.1831	-0.3545	-0.0107
			NMAD	0.3287	0.3374	0.3837	0.4271	0.5241	0.7543	1.4602	3.485	0.3967
			LoD	0.6574	0.6747	0.7674	0.8542	1.0483	1.5085	2.9204	6.971	0.7934
	forest	161235	Mean	-1.2516	-0.8826	-0.7077	-0.9167	-1.3524	-1.9558	-2.4073	-1.8772	-0.9312
			Stdev	2.0271	1.7148	1.6125	1.8158	2.149	2.4995	3.0035	3.4403	1.8302
			Median	-0.5654	-0.374	-0.2656	-0.3672	-0.665	-1.5244	-2.4394	-1.6797	-0.3672
			NMAD	0.8296	0.6747	0.64	0.8325	1.3233	2.3585	2.9942	3.8194	0.7775
			LoD	1.6592	1.3493	1.28	1.6649	2.6466	4.717	5.9883	7.6388	1.555
Pemdang Khola	bare rock	3866578	Mean	-0.021	0.0131	0.0423	0.0401	0.0414	0.0524	-0.0712	0.3663	0.0348
			Stdev	0.5465	0.6174	0.6483	0.6925	1.0499	1.9234	2.9747	3.8373	0.8838
			Median	-0.0518	-0.0195	0.0215	0.0234	0.0303	0.0478	0.0088	0.1514	0.0146
			NMAD	0.3026	0.3431	0.3721	0.3938	0.4894	0.8687	1.8663	3.3909	0.4054
			LoD	0.6052	0.6861	0.7442	0.7875	0.9788	1.7373	3.7326	6.7817	0.8108
	forest	94832	Mean	-0.3485	-0.2365	-0.1606	-0.0937	-0.0862	-0.0856	-0.2622	0.3373	-0.1149
			Stdev	0.7618	0.705	0.6297	0.6024	0.724	1.2261	2.0771	2.4854	0.7375
			Median	-0.2236	-0.1455	-0.1016	-0.0644	-0.0703	-0.0723	-0.1328	0.6465	-0.081
			NMAD	0.4032	0.3736	0.4097	0.4242	0.501	0.7688	1.6636	2.1269	0.4561
			LoD	0.8063	0.7471	0.8193	0.8484	1.002	1.5375	3.3272	4.2537	0.9122
Brematang Plain	bare rock	1225610	Mean	-0.0163	-0.0559	-0.2794	-0.6719	-2.0028	-2.5643	1.8555	5.9242	-0.3955
			Stdev	0.6846	1.5776	3.9012	6.7763	12.6711	19.713	26.005	27.5043	7.7955
			Median	0.002	0.0039	-0.0068	0.0664	0.081	-0.0205	-0.1621	0.9009	0.0156
			NMAD	0.3258	0.3649	0.4503	0.472	0.7399	2.069	4.9155	13.4093	0.4286
			LoD	0.6516	0.7297	0.9005	0.944	1.4798	4.138	9.8311	26.8186	0.8573
	forest	365329	Mean	-0.3943	-0.5842	-0.9618	-1.8393	-3.4345	-3.8199	-3.8642	-4.1128	-1.7902
			Stdev	4.8163	5.3953	6.087	6.6929	9.1157	9.345	9.7543	12.7909	7.2125
			Median	-0.0342	-0.124	-0.3828	-0.626	-1.1465	-1.8106	-2.2451	-3.0156	-0.4766
			NMAD	0.721	0.8702	1.277	1.8286	2.664	3.3532	3.9382	6.6977	1.61
			LoD	1.443	1.7404	2.553	3.6572	5.328	6.7065	7.8764	13.3954	3.219
Brematang Dam	bare rock	1478803	Mean	-0.3586	-0.0583	0.1618	0.209	0.0557	-0.1796	-0.7417	-0.8791	0.0528
			Stdev	3.074	3.1193	3.314	3.5805	4.1718	5.5027	6.984	9.6435	4.1618
			Median	-0.0273	0.0713	0.1494	0.1719	0.1377	0.084	-0.2959	-0.8257	0.1377
			NMAD	0.7688	0.7138	0.708	0.7992	0.9788	1.7953	3.5559	6.7803	0.9426
			LoD	1.5376	1.4275	1.416	1.5984	1.9576	3.5906	7.1118	13.5606	1.8852
	forest	1914430	Mean	-1.3554	-1.2676	-1.1417	-0.9053	-0.9599	-0.9006	-0.7186	-0.2426	-0.9479
			Stdev	6.2682	6.5328	6.7838	7.1377	8.0171	8.6833	9.3953	12.1345	7.9017
			Median	-0.3955	-0.3096	-0.1856	-0.0107	-0.0127	-0.166	-0.3594	-0.3115	-0.0918
			NMAD	2.8479	2.6554	2.1298	1.6636	2.095	3.275	4.6592	7.1032	2.4338
			LoD	5.6958	5.3107	4.2596	3.3271	4.19	6.55	9.3185	14.2064	4.8676

Reach	Landcover	Sample number/ Sample area	Statistics of DSM of difference	Slope (degrees)								
				0-10	10-20	20-30	30-40	40-50	50-60	60-70	70-90	All
Helambu Khola	bare rock	7236911	Mean	-0.0753	-0.0821	-0.094	-0.0684	-0.1543	-0.2264	-0.0959	1.2841	-0.0921
			Stdev	1.7005	1.7833	2.0863	2.0468	2.9844	4.4766	5.8918	7.3118	2.3595
			Median	-0.0107	0.0088	0.0273	0.0478	0.0518	0.0478	0.1182	1.3262	0.0322
			NMAD	0.3431	0.3388	0.3533	0.3837	0.5227	1.0757	2.6843	5.4106	0.3924
			LoD	0.6863	0.6775	0.7066	0.7674	1.0453	2.1514	5.3686	10.8211	0.7847
	forest	682600	Mean	-1.353	-0.907	-0.738	-0.5632	-0.7768	-1.1739	-1.4223	-0.8803	-0.8204
			Stdev	3.7814	3.3255	3.2599	3.1991	4.154	5.4876	6.8567	8.6921	4.3401
			Median	-0.2539	-0.124	-0.1133	-0.1289	-0.168	-0.2695	-0.5122	-0.3545	-0.1562
			NMAD	0.8673	0.5849	0.6327	0.6704	0.8861	1.7649	3.3858	5.9492	0.8948
			LoD	1.7346	1.1698	1.2653	1.3408	1.7722	3.5297	6.7716	11.8984	1.7895
Namsang Khola	bare rock	16035623	Mean	-0.0871	-0.1058	-0.1498	-0.1926	-0.3502	-0.6069	-0.7653	-0.3754	-0.2061
			Stdev	2.1778	2.3161	2.3574	2.6966	3.9931	5.8407	7.2955	9.4659	3.0653
			Median	0.0176	0.0068	-0.0166	-0.0156	0	0.041	0.0322	0.3652	-0.0068
			NMAD	0.3591	0.3706	0.3982	0.4459	0.6009	1.2611	3.0159	5.5127	0.446
			LoD	0.7182	0.7411	0.7964	0.8918	1.2017	2.5222	6.0319	11.0254	0.8921
	forest	6496690	Mean	0.1362	0.1458	0.1869	0.2565	0.4429	0.7099	1.0541	2.0152	0.4424
			Stdev	4.3945	4.325	4.252	4.2928	5.0207	5.9915	7.0476	8.6521	5.1214
			Median	-0.1631	-0.1377	-0.0752	-0.0176	0.1318	0.3799	0.7773	1.9277	0.0361
			NMAD	0.8151	0.8383	0.8745	0.9324	1.4768	2.7422	4.3595	6.5515	1.4145
			LoD	1.6301	1.6766	1.749	1.8647	2.9536	5.4843	8.719	13.1031	2.829
Melamchi Khola (lower reaches)	bare rock & farmland	11296665	Mean	-0.542	-0.6434	-0.6193	-0.5051	-0.3857	-0.3135	-0.3253	-0.1396	-0.5593
			Stdev	2.6686	1.9541	1.6709	1.9017	2.4285	3.1718	4.0634	5.383	2.1794
			Median	-0.6484	-0.6924	-0.6768	-0.5723	-0.4297	-0.291	-0.2266	0	-0.6367
			NMAD	0.9179	0.9614	1.0251	1.1974	1.5767	2.1558	2.8943	2.7451	1.0714
			LoD	1.8358	1.9227	2.0502	2.3949	3.1533	4.3115	5.7886	5.4902	2.1428
	forest	20554424	Mean	0.6717	0.6648	0.7131	0.7952	0.9143	1.0512	1.2286	1.539	0.8791
			Stdev	3.5705	3.4315	3.3591	3.4461	3.6973	4.1315	4.8571	6.292	3.8515
			Median	0.4609	0.4883	0.5615	0.6553	0.7656	0.8926	1.044	0.6279	0.669
			NMAD	1.7982	1.7722	1.7591	1.82	2.0342	2.4237	3.013	3.3967	2.0226
			LoD	3.5963	3.5443	3.5182	3.64	4.0683	4.8475	6.026	6.7934	4.0453

Erosion and deposition volumes derived from DSMs of difference on defined active areas.

Period	Reach*	(Raw data, Data filtered by slope- and landcover- dependent levels of detection)								
		Erosion			Deposition			Net change		
		Area [m^2]	Volume [m^3]	Mean elevation change [m]	Area [m^2]	Volume [m^3]	Mean elevation change [m]	Area [m^2]	Volume [m^3]	Mean elevation change [m]
Nov 2020-Oct 2021	Melamchi Khola (headwater)	(214582, 107179)	(-401991, -361786)	(-1.873, -3.376)	(172325, 60906)	(276962, 228800)	(1.607, 3.757)	(386907, 168085)	(-125029, -132986)	(-0.323, -0.791)
	Pemdang Khola	(791978, 496638)	(-6535628, -6365861)	(-8.252, -12.818)	(207572, 46803)	(223931, 165309)	(1.079, 3.532)	(999550, 543441)	(-6311697, -6200552)	(-6.315, -11.41)
	Bremathang Plain	(50237, 10551)	(-48951, -29920)	(-0.974, -2.836)	(745819, 676299)	(5435852, 5382469)	(7.288, 7.959)	(796056, 686850)	(5386901, 5352549)	(6.767, 7.793)
	Bremathang Dam	(1221837, 1166793)	(-48729015, -48619738)	(-39.882, -41.67)	(38125, 11752)	(88638, 60666)	(2.325, 5.162)	(1259962, 1178545)	(-48640377, -48559072)	(-38.605, -41.203)
	Helambu Khola	(542310, 204431)	(-1129591, -946753)	(-2.083, -4.631)	(276786, 40896)	(157020, 69948)	(0.567, 1.71)	(819096, 245327)	(-972571, -876805)	(-1.187, -3.574)
	Namsang Khola	(325859, 39622)	(-337708, -173189)	(-1.036, -4.371)	(225038, 23065)	(157787, 64103)	(0.701, 2.779)	(550897, 62687)	(-179921, -109086)	(-0.327, -1.74)
	Melamchi Khola (middle reaches)	(747014, 663177)	(-14661542, -14541374)	(-19.627, -21.927)	(119718, 51564)	(527896, 460406)	(4.409, 8.929)	(866732, 714741)	(-14133646, -14080968)	(-16.307, -19.701)
	Melamchi Khola (lower reaches)	(950564, 570741)	(-5290202, -4784017)	(-5.565, -8.382)	(2280556, 1857707)	(16738874, 16249440)	(7.34, 8.747)	(3231120, 2428448)	(11448672, 11465423)	(3.543, 4.721)
Oct 2021-Dec 2023	Melamchi Khola (headwater)	(111461, 45575)	(-108177, -84691)	(-0.971, -1.858)	(69673, 22999)	(43150, 28812)	(0.619, 1.253)	(181134, 68574)	(-65027, -55879)	(-0.359, -0.815)
	Pemdang Khola	(204202, 128085)	(-643545, -600011)	(-3.152, -4.684)	(265458, 180791)	(730543, 693527)	(2.752, 3.836)	(469660, 308876)	(86998, 93516)	(0.185, 0.303)
	Bremathang Plain	(66399, 29532)	(-227439, -213646)	(-3.425, -7.234)	(84797, 30371)	(56983, 39874)	(0.672, 1.313)	(151196, 59903)	(-170456, -173772)	(-1.127, -2.901)
	Bremathang Dam	(196822, 134675)	(-1005641, -953284)	(-5.109, -7.078)	(109931, 47473)	(250378, 205978)	(2.278, 4.339)	(306753, 182148)	(-755263, -747306)	(-2.462, -4.103)
	Helambu Khola	(39061, 10531)	(-41932, -30700)	(-1.074, -2.915)	(64555, 22194)	(48202, 32142)	(0.747, 1.448)	(103616, 32725)	(6270, 1442)	(0.061, 0.044)
	Namsang Khola	(2166, 222)	(-955, -245)	(-0.441, -1.104)	(3276, 430)	(1459, 468)	(0.445, 1.088)	(5442, 652)	(504, 223)	(0.093, 0.342)
	Melamchi Khola (lower reaches)	(1844102, 414259)	(-3292333, -1830602)	(-1.785, -4.419)	(1007409, 256782)	(1214679, 763641)	(1.206, 2.974)	(2851511, 671041)	(-2077654, -1066961)	(-0.729, -1.59)

* Melamchi Khola (middle reaches) is excluded from the DoD analysis of the period Oct 2021-Dec 2023 due to no visual change detected from orthoimages.